Palestinian Medical and Pharmaceutical Journal



The Design, Synthesis and Biological Evolution of Novel Pyrazole Derivatives as Potent Lung Cancer Agent

Ameer Hassan^{1,*}, Basma M. Abd Razik^{1,2} & Noor H. Naser³

(Type: Full Article). Received: 9th Jun. 2025, Accepted: 20th Sep. 2025 Published: xxxx DOI: xxxx

Accepted Manuscript, In Press

Abstract: Non-small-cell lung cancer (NSCLC) accounts for the majority of lung-cancer deaths, largely driven by dysregulated epidermal growth factor receptor (EGFR) signaling that promotes uncontrolled proliferation and survival. While EGFR tyrosine-kinase inhibitors (TKIs) have provided significant therapeutic benefit, challenges related to resistance and tolerability highlight the need for novel compounds with improved binding interactions and favorable drug-like characteristics. A novel series of pyrazole-based carbamothioyl compounds was synthesized and tested for their anticancer activity against non-small-cell lung carcinoma (NSCLC). The compounds were prepared via an ultrasound-assisted synthetic route involving acyl chloride formation, thiocyanation, and subsequent coupling with substituted aminopyrazoles. The structural features of the synthesized compounds were verified using FTIR, ¹H NMR, and ¹³C NMR techniques. Their cytotoxic behavior was evaluated in A549 lung cancer cells through the MTT method following incubation intervals of 24, 48, and 72 hours. All compounds exhibited dose- and time-dependent antiproliferative effects, with compounds H2 and H5 showing the highest potency at 72 hours, yielding IC₅₀ values of 11.88 and 12.49 µg/mL, respectively—both more active than the standard drug erlotinib (IC₅₀ = 13.53 µg/mL). Morphological evaluation revealed characteristic features of apoptosis and necrosis, including cell shrinkage and chromatin condensation. These findings indicate that all synthesized derivatives possess promising cytotoxic activity and promising lead compounds for further development in targeted lung cancer therapy.

Keywords: Pyrazole Derivatives, EGFR Inhibitors, NSCLC, Ultrasound-Assisted Synthesis, Cytotoxicity, A549 Cell Line.

Highlights

- Six novel pyrazole-based compounds were synthesized via an ultrasound-assisted protocol, incorporating thioamide and benzamide functionalities designed to enhance anticancer efficacy against NSCLC cells.
- All synthesized derivatives (H1–H6) demonstrated cytotoxicity against A549 lung cancer cells in a time- and dose-dependent manner, with compounds H2 and H5 outperforming erlotinib after 72 hours.
- Comprehensive structural elucidation using FT-IR, ¹H NMR, and ¹³C NMR confirmed the successful formation of the target compounds, revealing characteristic signals for amide, thiocarbonyl, and substituted pyrazole groups.
- Morphological assessments of treated A549 cells showed hallmark features of apoptosis and necrosis, including nuclear condensation, cell shrinkage, and membrane disintegration, indicating effective cytotoxic action.

Introduction

Cancer encompasses a group of diseases characterized by the uncontrolled growth of atypical cells that lose their normal functions, invade surrounding tissues, and spread to distant organs through blood or lymphatic pathways [1,2]. It remains a leading cause of mortality worldwide and poses significant healthcare challenges in both developed and developing regions. With nearly 82% of the global population living in low-income countries, the burden of cancer is expected to rise substantially, largely due to population aging [3]. Current

treatment strategies include surgical resection, radiotherapy, chemotherapy, and targeted molecular therapies such as immunotherapy and tyrosine kinase inhibitors. However, the effectiveness of these interventions varies with tumor type, stage, location, and patient condition [4,5]. While surgery and radiotherapy are effective for localized tumors, they often fail to control metastatic disease [6], underscoring the central role of chemotherapy. Nonetheless, the complex tumor microenvironment, cellular heterogeneity, similarity to normal cells, and the development of chemoresistance continue to limit the efficacy of existing anticancer therapies [7].

Lung cancer is the most lethal cancer globally, accounting for approximately 1.6 million deaths each year [8]. Non-small-cell lung cancer (NSCLC) represents about 85% of cases, with adenocarcinoma (LUAD) and squamous cell carcinoma (LUSC) as the predominant subtypes [9]. In regions with high smoking prevalence, tobacco use is the major etiological factor, responsible for more than 80% of lung cancer cases [10]. The molecular heterogeneity of NSCLC requires personalized treatment approaches; however, most patients are diagnosed at advanced stages (III or IV), where surgery is no longer curative, leaving radiotherapy and chemotherapy as the primary therapeutic options [11]

Heterocyclic scaffolds play a fundamental role in drug design because of their ability to influence both pharmacodynamic and pharmacokinetic properties. The incorporation of heteroatoms such as nitrogen, oxygen, or sulfur modifies electronic distribution, polarity, and molecular geometry, while also introducing additional hydrogen-bonding interactions. These

1

¹ Department of Pharmaceutical Chemistry, Faculty of Pharmacy, Mustansiriyah University, Baghdad, Iraq.

^{*} Corresponding author email: ameer_hassan@uomustansiriyah.edu.iq

² E-mail: basma_m.abd_razik@uomustansiriyah.edu.iq

³ Department of Pharmaceutical Chemistry, College of Pharmacy, Al-Zahraa University for Women, Karbala, Iraq. E-mail: noor.hatef@alzahraa.edu.iq

features often enhance solubility, metabolic stability, and selectivity, making heterocycles valuable bioisosteric replacements for phenyl and other aromatic groups. Consequently, heterocyclic systems are indispensable in optimizing drug-receptor interactions and ADME characteristics in modern medicinal chemistry [12]. Among these, the pyrazole scaffold—a five-membered heterocycle containing two adjacent nitrogen atoms-has emerged as a privileged motif due to its versatile reactivity and broad spectrum of biological activities [13]. Within the pyrazole ring, the nitrogen atom at position 1 (N1) resembles a pyrrolic nitrogen, as its lone pair participates in resonance, whereas the nitrogen at position 2 (N2) is pyridinic in nature and contributes to basicity, thereby enhancing the scaffold's ability to interact with biological targets [14]



Figure (1): The structure of pyrazole [14].

The distinctive electronic properties of the pyrazole core have been widely harnessed in the design of several FDA-approved drugs. Structure—activity relationship (SAR) studies demonstrate that substitutions at specific positions on the pyrazole ring can markedly influence anticancer potency [15]. Computational approaches, including molecular docking, are frequently used to predict ligand—receptor binding interactions, while scaffold-hopping strategies have aided in optimizing bioactivity profiles [16]. Pyrazole motifs are widely represented in FDA approved therapeutics, like celecoxib, a diaryl-pyrazole COX-2 inhibitor; zaleplon, a pyrazolopyrimidinone sedative-hypnotic; and modern anticancer agents such as the TRK inhibitors larotrectinib and entrectinib, which incorporate pyrazole-fused frameworks [17].

Recent research has underscored the broad anticancer potential of pyrazole-based compounds. Sivaramakarthikeyan et al. synthesized pyrazole-benzimidazole hybrids exhibited cellkilling effects on pancreatic cancer lines, achieving IC₅₀ values 30.9 ± 0.77 and 32.8 ± 3.44 μ M, outperforming the reference drug gemcitabine [18]. Similarly, Mohamady et al. developed novel diarylpyrazole derivatives that demonstrated remarkable antiproliferative effects against HepG2 cells, with compound 19 inducing G2/M phase arrest and apoptosis, achieving an IC50 of 0.083 µM [19]. Wang et al. reported pyrazole-naphthalene hybrids with enhanced cytotoxicity against MCF-7 breast cancer cells, where compound 20 exhibited a fivefold greater potency than cisplatin [20]. In lung cancer research, Kuthyala and colleagues synthesized heteroaromatic hybrids containing a pyrazole scaffold, that demonstrated selective antiproliferative effects on A549 cells without harming normal cell lines, with molecular docking studies indicating effective CDK2 inhibition [21]. Furthermore, Badithapuram et al. introduced phthalazinepiperazine-pyrazole conjugates with superior antiproliferative effects across several cancer cell types, notably A549 lung cancer cells, while showing limited harm to healthy cells [22]. Figure 2 illustrates representative examples of pyrazole derivatives with anticancer activity from the literature. Collectively, these findings highlight the versatility of the pyrazole scaffold in anticancer drug discovery and provide a strong

rationale for the continued investigation into pyrazole-based compounds as promising drug candidates continues to grow. In this pursuit A novel series of N-((5-phenyl-1H-pyrazol-3-yl)carbamothioyl)benzamide analogues were synthesized and have been extensively investigated for their potential to act as kinase inhibitors and anticancer agents. This synthetic strategy typically involves two key steps: the construction of a 5-phenyl-substituted pyrazole core, followed by the conjugation of a thio-benzamide moiety.[23].

In recent years, ultrasound-assisted organic synthesis (sonochemistry) has emerged as a green and efficient approach in medicinal chemistry. Ultrasound promotes cavitation, which enhances mass transfer, accelerates reaction rates, and often increases product yields under milder conditions compared to conventional heating. These features make ultrasound particularly attractive for multi-step heterocyclic synthesis, where efficiency and sustainability are crucial [24]. In the present study, ultrasound was employed in the coupling steps to afford the target pyrazole carbamothioyl derivatives, providing a rapid and environmentally friendly route to the designed molecules

Figure (2): Literature examples of anticancer pyrazole derivatives.

Building on the remarkable pharmacological potential of pyrazole-based compounds and the urgent need for innovative lung cancer therapies, the present study focuses on the design and biological evaluation of six newly synthesized pyrazole derivatives. These molecules were deliberately engineered with functional groups intended to enhance anticancer efficacy, with the goal of developing potent inhibitors selective for lung cancer cell lines. The synthesis, structural characterization, and preliminary cytotoxic evaluation of these derivatives are presented in the following sections.

Experimental Procedures

Chemistry

Reagents and Materials: All reagents and solvents were of analytical grade and used without further purification. Substituted benzoic acids, substituted pyrazoles, ammonium thiocyanate, thionyl chloride, acetonitrile, ethanol, and hydrochloric acid were obtained from commercial suppliers: Macklin (China), Sigma-Aldrich (USA), LOBA CHEMIE (India), and Honeywell (Germany). All chemicals were stored and handled according to the manufacturers' recommendations.

Instrumentation: Melting points were measured using a Stuart digital melting point apparatus (Stuart, UK) with open glass capillary tubes, and values are reported without correction. FT-IR spectra were acquired using a Shimadzu FTIR-8400S instrument (Japan), while ultrasonic-assisted reactions were conducted using a P200St device (Hielscher Ultrasonics,

Germany). NMR analyses were performed in DMSO-d₆ solvent using a Bruker 300 MHz spectrometer for proton (¹H) NMR and a Bruker 75 MHz instrument for carbon (¹³C) NMR (Bruker, USA). Chemical shifts (δ) are expressed in parts per million (ppm) with tetramethylsilane (TMS) as the internal reference. Coupling constants (J) are stated in hertz (Hz), and signal multiplicities are noted as: s (singlet), d (doublet), t (triplet), q (quartet), and m (multiplet).

General Synthetic Protocol for Compounds H1–H6: An equimolar amount (0.01 mol) of 4-substituted benzoic acid was dissolved in 1,2-dichloroethane and heated under reflux with thionyl chloride (2.36 g, 0.02 mol) until gas evolution ceased. After completion, the reaction mixture was subjected to reduced pressure distillation to eliminate residual solvent and excess reagent [25]. The resulting 4-substituted benzoyl chloride (0.01 mol) was then accurately transferred into 10 mL of anhydrous acetonitrile for subsequent use. To initiate the reaction and further enhance the outcome, precisely measured ammonium thiocyanate (0.01 mol) is added gradually in portions under stirring. The mixture is then subjected to sonication for a period of 15 minutes, employing sound waves at a specific frequency of 37 kHz, which ensures thorough and rapid reaction progress.

Following the sonication process, the resulting ammonium chloride is separated from the mixture through filtration process. Once the filtrate is obtained, the carefully selected and suitable amino pyrazole (0.01mol) is introduced to the raw benzoyl isothiocyanate solution, creating an optimal blend for the subsequent reactions. The mixture is then carefully exposed to sonication for a period of 25 minutes. To consolidate the reaction and facilitate the isolation of the desired compounds, the mixture is consequently poured into an accurately measured 50 mL of 0.1 M HCl solution, providing an ideal medium for further reaction progression. Finally, to obtain compounds 1-6H which was recrystallization form ethanol [26].

N-((5-(4-chlorophenyl)-1H-pyrazol-3-yl) carbamothioyl)-4-methoxy benzamide (H1): This compound was obtained in a yield of 77%, with a melting point of 253-255 °C. FT-IR analysis (cm⁻¹) displayed characteristic absorptions at: 3319 (N-H), 3280 (N-H, pyrazole), 3132 (N-H adjacent to C=S), 3055 (C-H, aromatic), 2953 and 2837 (C-H, aliphatic), 1654 (C=O, amide), 1502, 1483 (C=C, aromatic), 1261 and 1226 (C-O-C, methoxy), 1159 (C=S), and 813 (para-substituted ring). 1H NMR (DMSOd₆, δ ppm): 3.82 (s, 3H, OCH₃), 6.83 (s, 1H, pyrazole H), 7.07-7.10 (d, 1H, Ar-H near OCH₃), 7.73-7.75 (d, 2H, Ar-H ortho to CI), 7.96-7.99 (d, 2H, Ar-H meta to CI), 8.02-8.05 (d, 2H, Ar-H meta to OCH₃), 11.20 (s, 1H, NH-pyrazole), 11.27 (s, 1H, NH-C=O), 11.46 (s, 1H, NH-pyrazole). ¹³C NMR (DMSO-d₆, δ ppm): 55.73 (OCH₃), 93.20 (pyrazole CH), 114.93 (2C, Ar-CH, ring A), 126.69 (2C, Ar-CH, ring B), 129.22, 129.63 (Ar-CH, ring A), 130.08 (2C, Ar-C, ring B), 130.77, 134.43 (Ar-C, ring B), 143.89 (C-pyrazole linked to ring B), 150.69 (C-pyrazole), 161.25 (Ar-C, ring A), 164.33 (C=O), 177.64 (C=S).

Fluoro-N-((5-(4-fluorophenyl)-1H-pyrazol-3-yl)

carbamothioyl) benzamide (H2): This compound was isolated in 72% yield with a melting point of 243–245 °C. The FT-IR spectrum (cm $^{-1}$) exhibited bands at: 3277 (N–H), 3168 (N–H, pyrazole), 3108 (N–H close to C=S), 3070 (C–H, aromatic), 1670 (C=O, amide), 1598, 1563, 1501 (C=C, aromatic), 1304 (C–F), 1154 (C=S), and 837 (para-disubstituted aromatic). H NMR (DMSO-d₆, δ ppm): 7.30–7.42 (dd, 2H, Ar–H, ring A), 7.46 (s, 1H, pyrazole H), 7.79–7.84 (dd, 2H, Ar–H, ring B), 7.85–7.88 (dd, 2H, Ar–H, ring A), 8.08–8.11 (dd, 2H, Ar–H, ring B), 11.77 (s, 1H, NH–pyrazole), 13.15 (s, 1H, NH–C=O), 13.31 (s, 1H, NH–C=S).

 13 C NMR (DMSO-d₆, δ ppm): 96.16 (pyrazole CH), 115.81, 116.37 (2C, Ar–CH, ring A), 116.10, 116.66 (2C, Ar–C, ring B),

127.72, 127.82 (2C, Ar–C, ring B), 129.00 (C–pyrazole), 132.23 (C–pyrazole linked to ring B), 132.35 (Ar–C, ring B), 163.78 (C–F), 168.14 (C=O), 177.55 (C=S).

4-bromo-N-((5-(4-bromophenyl)-1H-pyrazol-3-yl) carbamothioyl) benzamide (H3)

This compound was isolated in 71% yield, with a melting point of 234–235 °C. The FT-IR spectrum (cm⁻¹) showed absorptions at: 3240 (N-H), 3200 (N-H in pyrazole), 3165 (N-H near C=S), 3026 (aromatic C-H), 1668 (amide C=O), 1610, 1541, 1481 (C=C aromatic), 1188 (C=S), and 813.96 (parasubstitution band).

¹H NMR (DMSO-d₆, δ ppm): 7.47 (s, 1H, pyrazole proton), 7.62–7.64 (dd, 2H, Ar–H, ring B), 7.65–7.67 (dd, 2H, Ar–H, ring A), 7.69–7.72 (dd, 2H, Ar–H, ring B), 7.87–7.90 (dd, 2H, Ar–H, ring A), 11.77 (s, 1H, NH–pyrazole), 13.15 (s, 1H, NH–C=O), 13.31 (s, 1H, NH–C=S). ¹³C NMR (DMSO-d₆, δ ppm): 96.46 (CH, pyrazole), 121.94 (Ar–C, ring A), 127.54 (Ar–C, ring B), 127.66 (2C, Ar–CH, ring A), 129.63 (2C, Ar–CH, ring B), 131.29, 131.66, 131.90 (Ar–CH, ring A), 132.47 (Ar–C, ring B), 140.50 (pyrazole C), 154.62 (pyrazole C linked to ring B), 168.37 (C=O), 177.49 (C=S, thiocarbonyl group).

N-((5-(4-chlorophenyl)-1H-pyrazol-3-yl) carbamothioyl)-4-methyl benzamide (H4): The compound H4 was obtained in 67% yield and exhibited a melting point of 243–245 °C. Infrared absorption bands (cm $^{-1}$): 3363 (N–H), 3195 (N–H, pyrazole), 3159 (N–H adjacent to C=S), 3065 (aromatic C–H), 2923 and 2857 (aliphatic C–H), 1666 (amide C=O), 1608, 1571, 1503 (C=C aromatic), 1195 (C=S), and 832 (para-disubstitution on ring). 1 H NMR (DMSO-d₆, 5 ppm): 2.37 (s, 3H, CH₃ group), 7.33–7.36 (dd, 2H, Ar–H, ring A), 7.49 (s, 1H, pyrazole proton), 7.52–7.55 (dd, 2H, Ar–H, ring B), 7.80–7.87 (dd, 2H, Ar–H, ring A), 7.91–7.94 (dd, 2H, Ar–H, ring B), 10.84 (s, 1H, NH–pyrazole), 11.56 (s, 1H, NH–C=O), 13.22 (s, 1H, NH–C=S).

¹³C NMR (DMSO-d₆, δ ppm): 21.61 (CH₃, benzylic), 96.47 (pyrazole CH), 127.30, 129.32, 129.48, 129.56 (Ar–CH, rings A & B), 130.90, 132.36, 133.31, 140.54 (Ar–C), 144.22 (pyrazole C), 151.08 (pyrazole C attached to ring A), 169.01 (C=O, amide), 177.71 (C=S).

N-((5-(4-methoxyphenyl)-1H-pyrazol-3-yl)

carbamothioyl)-4-methylbenzamide (H5): This compound was obtained in 70% yield with a melting point of 203–204 °C. The FT-IR spectrum (cm⁻¹) exhibited bands at 3195 (N–H), 3165 (N–H, pyrazole), 3113 (N–H near C=S), 3077 (aromatic C–H), 2950, 2923, and 2862 (aliphatic C–H), 1668 (amide C=O), 1569, 1564, 1502 (C=C, aromatic), 1250, 1122 (C–O–C for methoxy), 1177 (C=S), and 834 (indicative of para-substitution).

¹H NMR (DMSO-d₆, δ ppm): 2.40 (s, 2H, CH₃ of tolyl group), 3.80 (s, 2H, OCH₃), 7.02–7.05 (dd, 2H, Ar–H, ring B), 7.34 (s, 1H, pyrazole H), 7.34–7.36 (dd, 2H, Ar–H, ring A), 7.68–7.70 (dd, 2H, Ar–H, ring B), 7.91–7.94 (dd, 2H, Ar–H, ring A), 11.58 (s, 1H, NH-pyrazole), 13.15 (s, 1H, NH adjacent to C=O), 13.23 (s, 1H, NH next to C=S). ¹³C NMR (DMSO-d₆, δ ppm): 21.61 (methyl, benzylic), 55.69 (methoxy), 95.26 (CH of pyrazole), 114.93 (2C, Ar–CH, ring B), 122.73 (Ar–C, ring B), 127.00 (2C, Ar–CH, ring B), 129.32, 129.48 (2C each, Ar–CH, ring A), 133.31 and 140.54 (Ar–C, ring A), 144.22 (pyrazole C), 151.09 (pyrazole C attached to Ar), 159.80 (C–O–C, methoxy), 169.01 (amide C=O), and 177.71 (C=S group).

N-((5-(4-methoxyphenyl)-1H-pyrazol-3-yl)

carbamothioyl)-4-nitrobenzamide (H6): This compound was isolated in 67% yield and had a melting point range of 266–267 °C. FT-IR (cm⁻¹): 3373 (N-H), 3228 (N-H in pyrazole), 3180 (N-H close to thiocarbonyl), 3070 (C-H aromatic), 2954 and 2880 (C-H aliphatic), 1674 (C=O amide), 1591, 1519, 1544

(C=C aromatic), 1342 (NO₂ asymmetric/symmetric), 1180 (C=S), and 831 (para-disubstitution).

 1 H NMR (DMSO-d₆, δ ppm): 3.76 (s, 3H, methoxy), 6.98–7.01 (dd, 2H, Ar–H, ring A), 7.35 (s, 1H, pyrazole proton), 7.64–7.67 (dd, 2H, Ar–H, ring B), 8.12–8.15 (dd, 2H, Ar–H, ring A), 8.28–8.31 (dd, 2H, Ar–H, ring B), 12.02 (s, 1H, NH–pyrazole), 12.95 (s, 1H, NH near C=O), 13.17 (s, 1H, NH next to C=S). 13 C NMR (DMSO-d₆, δ ppm): 55.66 (OCH₃), 95.53 (pyrazole CH), 114.89 (2C, Ar–CH, ring A), 122.12 (2C, Ar–CH, ring B), 123.74 (Ar–C, ring A), 127.02 (2C, Ar–CH, ring A), 130.75 (2C, Ar–CH, ring B), 138.37 (Ar–C, ring B), 142.56 (pyrazole C), 147.76 (Ar–C, NO₂ substituted), 150.22 (pyrazole C attached to ring B), 159.80 (methoxy-substituted aromatic C–O–C), 167.69 (C=O), and 176.98 (C=S).

Figure (3): Chemical structures of the synthesized pyrazole derivatives (H1–H6).

Evaluation of biological activity

Cell Culture Conditions: The A549 cell line, originating from human lung adenocarcinoma, was sourced from the Pasteur Institute's National Cell Bank (Iran). Cells were cultivated in RPMI-1640 medium (Gibco, USA), enriched with 10% fetal bovine serum (FBS), and supplemented with penicillin (100 U/mL) and streptomycin (100 $\mu g/mL$). Cultures were maintained at 37 °C in an incubator with 5% CO $_2$ and high humidity. Routine passaging was performed using trypsin–EDTA, and phosphate-buffered saline (PBS) was employed for washing and handling procedures [27].

Evaluation of Cytotoxicity via MTT Assay: The cytotoxic potential of compounds H1-H6 was investigated using the MTT [3-(4,5-dimethylthiazol-2-yl)-2,5employing diphenyltetrazolium bromide] reagent from Sigma-Aldrich. Cells were trypsinized, counted, and dispensed into 96-well plates at a density of 1.4 × 10⁴ cells/well in 200 µL of fresh RPMI medium. After a 24-hour incubation period for attachment, various concentrations of each compound (ranging from 3.125 to 50 μg/mL) were introduced. All compounds were prepared in DMSO. Incubation durations were 24, 48, and 72 hours at 37 °C in an atmosphere of 5% CO₂. At the end of each treatment period, the culture medium was removed, and 200 µL of MTT solution (0.5 mg/mL in PBS) was added to each well. The plates were returned to the incubator for 4 hours. After incubation, the MTT reagent was discarded, and 100 µL of DMSO was used to solubilize the resulting formazan crystals. Absorbance was measured at 570 nm using a microplate reader (ELISA reader, Model Wave XS2, BioTek, USA) [28].

Data Interpretation: Cell viability was calculated as a percentage relative to untreated control wells, which were assigned a baseline of 100% viability. Growth inhibition for each tested compound was calculated by subtracting the measured viability percentage from 100 [29]. The half-maximal inhibitory concentration (IC_{50}) for each derivative—defined as the dose necessary to reduce viability by 50%—was calculated from

dose–response plots using nonlinear regression [30]. These were constructed using both GraphPad Prism and OriginLab Pro software, and separate IC_{50} values were obtained at 24, 48, and 72-hour intervals. Erlotinib, a known EGFR inhibitor, was included as a positive benchmark. All experiments were repeated in triplicate, and average values are reported.

Statistical analysis: All experiments were performed in triplicate (n = 3) and repeated independently at least three times. The results are presented as mean \pm standard deviation (SD). Dose–response curves were generated, and IC_{50} values were calculated by non-linear regression using GraphPad Prism version 9.0 (GraphPad Software, San Diego, CA, USA). Statistical comparisons between treatment groups were conducted using one-way analysis of variance (ANOVA), followed by Tukey's post hoc test to determine significant differences. A value of p < 0.05 was considered statistically significant.

Results and discussion

Chemistry

Ultrasound-assisted organic synthesis has become a valuable tool for green chemistry due to its benefits such as shorter reaction durations, improved yields, and reduced energy requirements (Rao et al., 2015). In alignment with environmentally sustainable methods, six novel pyrazole derivatives (H1–H6) were synthesized through an ultrasonic approach.

The synthetic route (Scheme 1) began with the transformation of 4-substituted benzoic acids into their respective acid chlorides using thionyl chloride under reflux. These intermediates were then reacted with ammonium thiocyanate in acetonitrile to form benzoyl isothiocyanates. Lastly, the desired compounds were obtained by coupling these intermediates with substituted aminopyrazoles under ultrasonic conditions. The structural characteristics of the final compounds (H1-H6) were determined through melting point analysis and relevant functional groups came from FT-IR signatures. Complete structural confirmation was then provided by ¹H-NMR data and corroborating ¹³C-NMR results drawn from Silverstein's reference [31].

R1 = OCH3, Cl, F, Br R2 = F, NO2, CH3, Br, OCH3

Scheme (1): General scheme for synthesis.

The structures of compounds H1–H6 were confirmed by FT-IR spectroscopy through characteristic absorptions. N–H stretching bands for the amide, pyrazole, and thioamide groups appeared in the ranges of 3195–3373 cm $^{-1}$, 3165–3280 cm $^{-1}$, and 3108–3180 cm $^{-1}$, respectively. The amide C=O stretch was observed between 1654–1674 cm $^{-1}$, while the thiocarbonyl (C=S) appeared at 1020–1074 cm $^{-1}$. Aromatic C=C vibrations were recorded in the 1483–1598 cm $^{-1}$ range. The 1 H NMR spectra of compounds H1–H6 showed characteristic singlets in the δ 10.8–13.3 ppm range, corresponding to three distinct N–H protons: the amide N–H (near C=O), the pyrazole ring N–H, and the thioamide N–H. The pyrazole ring proton was consistently observed as a singlet near δ 6.83–7.5 ppm. Aromatic protons

appeared as doublet of doublets in the δ 6.98–8.31 ppm region, reflecting the substituted benzene rings on both aryl groups. The 13 C NMR spectroscopy of all compounds exhibited a distinct amide carbonyl (C=O) carbon appeared in the range of δ 164.33–170.33 ppm, while the thiocarbonyl (C=S) carbons were detected between δ 176.98–178.59 ppm, The protonated pyrazole carbon (CH) was consistently observed between δ 93.20–97.67 ppm. Accordingly, the structural integrity and successful synthesis of the pyrazole derivatives H1–H6 were comprehensively verified through FTIR, ¹H NMR, and 13 C NMR spectral analyses. The observed characteristic absorption bands, proton and carbon chemical shifts, and resonance patterns collectively substantiated the presence of incorporation of functional groups and affirmed the designed molecular architectures.

Table (1): Substituent patterns and definitions of intermediates (1–4) and final pyrazole derivatives (H1–H6).

Name of compound	R ₁	R ₂
1a	CI	
1b	F	
1c	Br	
1d	OCH₃	
H1	CI	OCH3
H2	F	F
H3	Br	Br
H4	CI	CH₃
H5	OCH₃	CH₃
H6	OCH₃	NO ₂

Assessment of Cytotoxic Potential

In Vitro Cell Survival Assay: The anti-proliferative effects of the synthesized pyrazole derivatives H1–H6 were evaluated for anti-proliferative activity on A549 cells using the MTT colorimetric assay; cell viability was calculated relative to untreated controls, and IC_{50} values were derived from non-linear regression of log-dose–response curves, the cytotoxicity was assessed against A549 non-small cell lung carcinoma cells across three different exposure durations 24, 48, and 72 hours.

The antiproliferative activity was determined by estimating the IC_{50} values, which represent the compound concentration required to inhibit 50% of cellular viability.

Erlotinib, an FDA-approved EGFR inhibitor, was used as a reference standard to compare the activity of the test compounds. Nonlinear regression analysis of dose–response curves produced IC $_{50}$ values, these findings are summarized and visually represented in Figures 4 to 6. A consistent, time-dependent increase in cytotoxicity was noted for all compounds, with IC $_{50}$ values typically decreasing with longer exposure times. This pattern emphasizes the significance of extended incubation to enhance anti-cancer effectiveness.

Cytotoxicity Profiles and Comparative Potency: All synthesized compounds demonstrated anti-proliferative activities in a time- and concentration-dependent manner. After 72 hours of treatment, IC $_{50}$ values for the derivatives ranged between 11.88 and 33.75 µg/mL, confirming their cytotoxic efficacy at micromolar concentrations. Notably, compounds H2 and H5 demonstrated the strongest cytotoxic response, exhibiting IC $_{50}$ values of 11.88 µg/mL and 12.49 µg/mL, respectively, surpassing the reference drug Erlotinib (IC $_{50}$ = 13.53 µg/mL).

This superior potency suggests that H2 and H5 may possess favorable cellular permeability or enhanced interactions with molecular targets within cancer cells. Compounds H1 and H3 exhibited moderate cytotoxic response IC $_{50}$ values of 14.65 and 25.75 μ g/mL, respectively.

Compounds H1 activity, showed cytotoxicity near that of Erlotinib. while compounds H4 and H6, for which the IC50 is slightly higher than that of erlotinib at 72 hours.

The IC_{50} profiles were corroborated by dose–response curves (Figures 4), which clearly illustrate the enhanced cytotoxic effect of synthesized compounds at lower concentrations and extended exposure times.

Cell Death Percentage Analysis: To complement the IC_{50} data, cell death percentages were determined at multiple concentrations, time points and illustrated figure 5. These results confirmed the cytotoxic trends observed in the IC_{50} analyses. At the highest tested concentration (50 µg/mL, 72h), compound H2 induced approximately 80% cell death, surpassing the effect of Erlotinib (~70%). Compounds H5 and H1 followed closely, inducing ~76% and ~71% cell death, respectively. This enhanced cell-killing efficacy further emphasizes the therapeutic potential of H2 and H5. Moreover, the performance of H1 underscores its promise as a competitive candidate to Erlotinib in terms of anti-lung cancer activity.

Morphological Changes of A549 Cell Line after Treatment with the Synthesized Compounds: Microscopic evaluation revealed pronounced morphological alterations in A549 cells following treatment with the synthesized pyrazole derivatives (H1–H6) across different concentrations (3.125–50 µg/mL) after 72 hours in compare to the untreated control, the exposed cells exhibited a progressive decrease in cell viability and monolayer integrity in a concentration-dependent manner.

At lower concentrations (3.125–12.5 µg/mL), initial signs of cytotoxicity were evident, including reduced cell density, early cell rounding, and partial detachment from the culture surface. As the concentration increased (25–50 µg/mL), more severe morphological changes were observed, characterized by significant cellular shrinkage, membrane blebbing, cytoplasmic granulation, and nuclear condensation. Furthermore, the formation of apoptotic bodies and loss of intercellular connections became more prominent. The treated cells exhibited a transition from the typical epithelial-like morphology of A549 cells to a more rounded, irregular appearance with increased floating dead cells, suggesting apoptosis and necrosis induction [32].

The extent of morphological disruption correlated with the increase in drug concentration, indicating a dose-dependent cytotoxic effect of the synthesized compounds [33]. These observations are consistent with the cytotoxic potential demonstrated in the MTT assay results, suggesting that the tested pyrazole derivatives effectively compromise A549 cell survival through the induction of cellular stress and apoptotic pathways. Morphological changes of A549 cells treated with pyrazole derivatives (H1–H6) and reference drug (R) at different concentrations for 72 hours compared to untreated control.

Structure-Activity Relationship (SAR) Analysis

The anticancer activity of the synthesized pyrazole derivatives (H1-H6) revealed clear structure-activity relationships in relation to the nature and position of substituents on the aromatic moiety as well as their lipophilic balance. Compounds bearing electron-donating groups, particularly methoxy and methyl substituents (H2 and H5), demonstrated superior cytotoxic activity with lower IC₅₀ values, suggesting that these groups enhance electronic density on the aromatic ring, thereby favoring stronger interactions with the EGFR binding pocket. In addition, these substituents increase lipophilicity, which can facilitate membrane permeability and improve Conversely, intracellular drug availability. derivatives incorporating electron-withdrawing substituents such as nitro

(H6) or halogen (H3, H4) showed comparatively weaker activity, which may be attributed to excessive polarity or reduced lipophilic character, impairing both receptor binding and cellular uptake. Interestingly, the unsubstituted analogue H1 exhibited only moderate inhibition, indicating that substitution on the phenyl ring is crucial for enhancing biological activity. Collectively, these findings underscore the dual role of electronic effects and lipophilicity in shaping the anticancer potential of the series, with para-positioned electron-donating substituents conferring optimal lipophilic balance and biological efficacy.

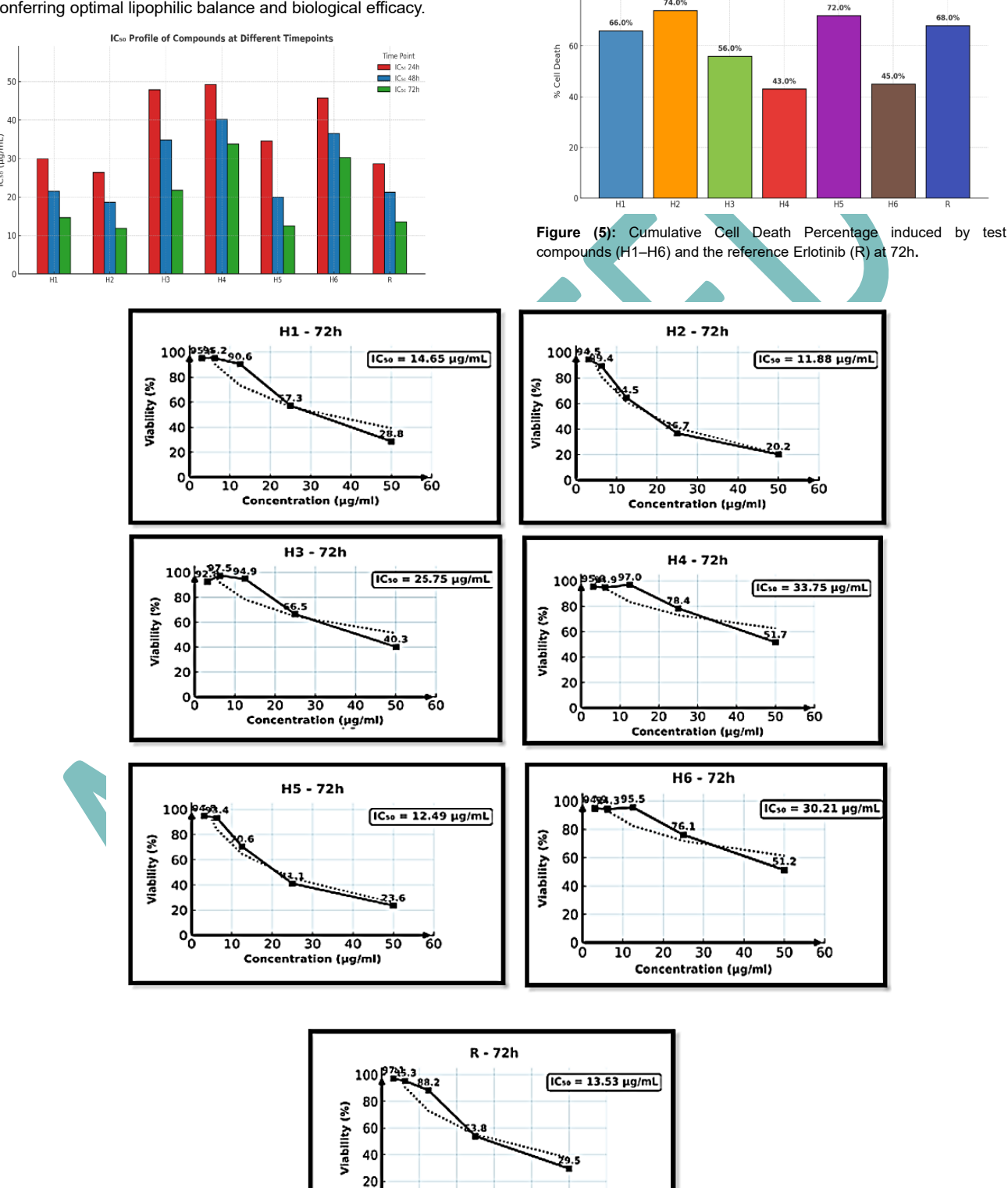


Figure (6): Dose–response cytotoxicity curves of pyrazole carbamothioyl derivatives (H1–H6) and reference drug (R, Erlotinib) against A549 lung cancer cells after 72 h treatment. IC₅₀ values are indicated on each plot.

Concentration (µg/ml)

20 30 40

Figure (4): Comparative Time-Dependent IC_{50} Profiles. The IC_{50} values (μ g/mL) of the synthesized pyrazole derivatives (H1–H6) in comparison

with the reference drug erlotinib (R) following 24, 48, and 72 hours of

treatment against A549 lung cancer cells. The results exhibit a clear trend

of decreasing IC_{50} values over time, highlighting the enhanced cytotoxic

% Cell Death at 72h for All Compounds

efficacy of the compounds with extended exposure durations.

Conclusion

In this study, six novel N-((5-aryl-1H-pyrazol-3-yl)carbamothioyl) benzamide derivatives (H1-H6) were successfully synthesized through an environmentally benign, ultrasound-assisted three-step protocol that converted readily available 4-substituted benzoic acids into benzoyl isothiocyanates and subsequently coupled them with aminopyrazoles. The structures were confirmed by FT-IR, 1H NMR, and ¹³C NMR spectroscopy, which verified the introduction of amide, thiocarbonyl, and pyrazole functionalities into the final products. In vitro cytotoxicity assays against A549 lung cancer cells demonstrated that all compounds exerted dose- and timedependent inhibitory effects, with H1, H2 and H5 showing the highest potency after, marginally surpassing the reference drug erlotinib under the same conditions. These results highlight the importance of para-substituent electronic effects on the thiocarbonyl-pyrazole core in modulating activity. The combination of synthetic accessibility, favorable structural features, and preliminary cytotoxic efficacy identifies H1, H2 and H5 as promising lead candidates. While no in vivo safety or resistance assays were included in the current study, the findings establish a strong foundation for further mechanistic exploration, optimization of substituents, and preclinical evaluation.

Disclosure Statements

- Ethics approval and consent to participate: The Institutional Ethical Committee- Department of
- Pharmacy, al Mustansiriyah University reviewed and approved the protocol.
- Consent for publication: All authors have read and approved the final version of the manuscript and consent to its publication in the journal.
- Availability of data and materials: Supplementary data can be shared upon
- request
- Author's contribution: Ameer Hassan carried out the synthesis of the target compounds, data collection, experimental work, data analysis, and preparation of the initial manuscript draft. Basma M. Abd Razik and Noor H. Naser provided scientific supervision, critical manuscript revision, and final approval of the version to be published.
- Competing interest: The authors have no conflict of interest to declare.
- Funding: This research received no specific grant from any funding agency.
- Acknowledgments: I would like to express my gratitude to the department of pharmaceutical chemistry at the College of Pharmacy/Mustansiriyah University (www.uomustansiriyah.edu.iq) Baghdad, Iraq, for their assistance with this project.

Open Access

This article is licensed under a Creative Commons Attribution 4.0 International License, which permits use, sharing, adaptation, distribution and reproduction in any medium or format, as long as you give appropriate credit to the original author(s) and the source, provide a link to the Creative Commons licence, and indicate if changes were made. The images or other third-party material in this article are included in the article's Creative Commons licence, unless indicated otherwise in a credit line to the material. If material is not included in the article's Creative Commons licence and your intended use is not permitted by statutory regulation or exceeds the permitted use, you will need to obtain permission directly from the copyright

holder. To view a copy of this license, visit https://creativecommons.org/licenses/by-nc/4.0/

References

- Rang HP, Dale MM, Ritter JM, Flower RJ. Anticancer drugs.
 In: Rang HP, Dale MM, Ritter JM, Flower RJ, editors. Rang
 Dale's Pharmacology. 8th ed. Edinburgh: Churchill Livingstone; 2016. p. 676–690.
- 2] Torre LA, Bray F, Siegel RL, Ferlay J, Lortet-Tieulent J, Jemal A. Global cancer statistics, 2012. CA Cancer J Clin. 2015;65(2):87–108. doi:10.3322/caac.21262.
- 3] American Cancer Society. Cancer Facts & Figures 2024 [Internet]. Atlanta (GA): American Cancer Society; 2024 [cited 2025 Jun 12]. Available from: https://www.cancer.org/research/cancer-facts-statistics/all-cancer-facts-figures.html
- 4] Haidar F, Mahdi MF, Khan AK. Synthesis, molecular docking, characterization, and preliminary evaluation of some new 1,3-diazetidin-2-one derivatives as anticancer agents. Al Mustansiriyah J Pharm Sci. 2024;24(1):48–58. doi:10,32947/ajps. v24i1.1026
- 5] Alberg AJ, Brock MV, Ford JG, Samet JM, Spivack SD. Epidemiology of lung cancer: diagnosis and management of lung cancer: American College of Chest Physicians evidence-based clinical practice guidelines. *Chest*. 2013;143(5 Suppl): e1S-e29S. doi:10.1378/chest.12-2345.
- 6] Herbst RS, Morgensztern D, Boshoff C. The biology and management of non-small cell lung cancer. *Nature*. 2018;553(7689):446–54. doi:10.1038/nature25183 IF: 48.5 Q1 B1.
- 7] Wilkinson L, Gathani T. Understanding breast cancer as a global health concern. *Br J Radiol*. 2022;95(1135):20211045. doi:10.1259/bjr.20211045.
- 8] Tsuda H, Uemura T. Accumulation of genetic and epigenetic alterations in normal cells and cancer risk. *NPJ Precis Oncol*. 2019; 3:7. doi:10.1038/s41698-019-0080-5.
- 9] Huang CY, Jang DT, Chen CF, Reddy MP, Bharath KV. Effects of current chemotherapy drugs and natural agents in treating non-small cell lung cancer: a review. *BioMedicine*. 2017;7(4):23–31. doi: 10.1016/j.biomed.2017.10.001.
- 10] Kim K, Kim D. Past, present, and future of anticancer nanomedicine. *Int J Nanomedicine*. 2020; 15:5719–43. doi:10.2147/IJN.S259857.
- 11] Joo WD, Visintin I, Mor G. Targeted cancer therapy—are the days of systemic chemotherapy numbered? *Maturitas*. 2013;76(4):308–14. doi: 10.1016/ j. maturitas. 2013. 09.008.
- 12] Martins PR, Spengler G, de Carvalho L. Heterocyclic anticancer compounds: recent advances. *Curr Top Med Chem.* 2015;15(4):291–308.
- 13] Kaur R, Dwivedi AR, Kumar B, Singh S, Kumar V. Recent advances in the medicinal chemistry of heterocyclic scaffolds as anti-inflammatory agents: a comprehensive review. Eur J Med Chem. 2017; 143:897–936. doi: 10.1016/j.ejmech.2017.12.033.
- 14] Ansari A, Ali A, Asif M, Shamsuzzaman. Biologically active pyrazole derivatives. *New J Chem.* 2017;41(1):16–41. doi:10.1039/C6NJ03181A.
- 15] Zhang Y, Wu C, Zhang N, Fan R, Ye Y, Xu J. Recent advances in the development of pyrazole derivatives as anticancer agents. *Int J Mol Sci.* 2023;24(16):12724.

- 16] Ibrahim ZN, Khan AK, Hamdi MD, Mehde AA. Drug design and in silico profiling of new pyrrole derivatives: promising anticancer agents against acute myeloid leukemia. *AI Mustansiriyah J Pharm Sci.* 2024;24(3):252–63. doi:10.32947/ajps. v24i3.1063.
- 17] Li G, Han C, Song C, Huang N, Du Y. Pyrazole-containing pharmaceuticals: target, pharmacological activity, and SAR studies. RSC Med Chem. 2022;13.
- 18] Sivaramakarthikeyan R, Shanmugam I, Vadivel S, Lim WM, Mai CW, Ramalingan C. Molecular hybrids integrated with benzimidazole and pyrazole structural motifs: design, synthesis, biological evaluation and molecular docking studies. ACS Omega. 2020;5(17):10089–98. doi:10.1021/acsomega.0c00630
- 19] Mohamady S, Ismail MI, Mogheith SM, Attia YM, Taylor SD. Discovery of 5-aryl-3-thiophen-2-yl-1H-pyrazoles as a new class of Hsp90 inhibitors in hepatocellular carcinoma. *Bioorg Chem.* 2020; 94:103433. doi: 10.1016/j.bioorg.2019.103433.
- 20] Wang GC, Liu WJ, Peng ZY, Huang Y, Gong ZP, Li YJ. Design, synthesis, molecular modelling and biological evaluation of pyrazole-naphthalene derivatives as potential anticancer agents on MCF-7 breast-cancer cells by inhibiting tubulin polymerization. *Bioorg Chem.* 2020; 103:104141. doi: 10.1016/j.bioorg.2020.104141.
- 21] Kuthyala S, Sheikh S, Prabhu A, Rekha PD, Karikannar NG, Shankar MK. Synthesis, characterization and anticancer studies of some pyrazole-based hybrid heteroatomics. *ChemistrySelect*. 2020;5(35):10827–34. doi:10.1002/slct.20200248.
- 22] Badithapuram V, Nukala KS, Dasari G, Thirukovela SN, Bandari S. Synthesis of new phthalazine-piperazine-pyrazole conjugates: in-vitro anticancer, ADMET and molecular docking studies. *ChemistrySelect.* 2023;8(10): e202204329. doi:10.1002/slct.202204329.
- 23] Badr MH, Hamed AR, El-Hady MA. Microwave-assisted synthesis of novel pyrazole-based thiourea derivatives and their antiproliferative evaluation. *J Heterocycl Chem.* 2022;59(5):1044–52.
- 24] Mohammadi Ziarani G, Kheilkordi Z, Gholamzadeh P. Ultrasound-assisted synthesis of heterocyclic compounds.

- Mol Divers. 2020;24(3):771-820. doi:10.1007/s11030-019-09964-1.
- 25] Nitulescu GM, Matei L, Aldea IM, Draghici C, Olaru OT, Bleotu C. Ultrasound-assisted synthesis and anticancer evaluation of new pyrazole derivatives as cell-cycle inhibitors. *Arab J Chem.* 2019;12(6):816–24.
- 26] Rao MS, Haritha M, Chandrasekhar N, Basaveswara Rao MV, Pal M. Ultrasound-mediated synthesis of 6-substituted 2,3-dihydro-1H-pyrrolo[3,2,1-ij] quinoline derivatives and their pharmacological evaluation. *Arab J Chem.* 2015. doi: 10.1016/j.arabjc.2015.05.013.
- 27] Shi Y, Tang B, Yu PW, Tang B, Hao YX, Lei X, et al. Autophagy protects against oxaliplatin-induced cell death via ER stress and ROS in Caco-2 cells. *PLoS One*. 2012;7(11): e51076. doi: 10.1371/journal.pone.0051076.
- 28] Kaplan A, Akalin Ciftci G, Kutlu HM. The apoptotic and genomic studies on A549 cell line induced by silver nitrate. *Tumor Biol.* 2017;39(4):1010428317695939. doi:10.1177/1010428317695939.
- 29] Chang J, Ren H, Zhao M, Chong Y, Zhao W, He Y, et al. Development of novel 4-anilinoquinazoline derivatives possessing quinazoline skeleton: design, synthesis, EGFR kinase inhibitory efficacy and in vitro anticancer activity. *Eur J Med Chem*. 2017; 138:669–88. doi: 10.1016/j.ejmech.2017.07.047.
- 30] Shaaban OG, Abd El Razik HA, Shams El-Dine A, Ashour FA, El-Tombary AA, Afifi OS, et al. Purines and triazolo[4,3-e] purines containing pyrazole moiety as potential anticancer and antioxidant agents. *Future Med Chem.* 2018;10(12):1449–64. doi:10.4155/fmc-2018-0089.
- 31] Silverstein RM, Webster FX, Kiemle DJ. Spectrometric Identification of Organic Compounds. 7th ed. Hoboken (NJ): Wiley-Interscience; 2005.
- 32] Sharma N, Arya G, Kumari R, Gupta N, Nimesh S. Evaluation of anticancer activity of silver nanoparticles on A549 human lung carcinoma cells through Alamar Blue assay. *Bio Protoc*. 2019;9(1): e3149. doi:10.21769/BioProtoc.3149.
- 33] Sebaugh JL. Guidelines for accurate EC50/IC50 estimation. *Pharm Stat.* 2011;10(2):128–34. doi:10.1002/pst.426.